J|A|C|S
ARTICLES
Published on Web 03/22/2003

Pressure-Induced Cation Migration and Volume Expansion in the Defect Pyrochlores $ANbWO_6$ ($A = NH_4^+$, Rb^+, H^+, K^+)

Paris W. Barnes,[†] Patrick M. Woodward,*[,†] Yongjae Lee,[‡] Thomas Vogt,[‡] and Joseph A. Hriljac[§]

Contribution from the Department of Chemistry, The Ohio State University, Columbus, Ohio, 43210, the Physics Department, Brookhaven National Laboratory, Upton, New York 11973-5000, and the School of Chemical Sciences, University of Birmingham, Birmingham B15 2TT, U.K.

Received November 4, 2002; E-mail: woodward@chemistry.ohio-state.edu

Abstract: The structural and compositional evolution of four members of the $ANbWO_6$ ($A = NH_4^+$, Rb^+, H^+, K^+) defect pyrochlore family have been studied as a function of pressure up to 7 GPa, using a diamond anvil cell and monochromatic synchrotron X-ray powder diffraction. In response to increasing hydrostatic pressure, NH_4NbWO_6 and $RbNbWO_6$ both initially contract but then undergo a fairly abrupt increase in their unit cell volumes above a characteristic threshold pressure. NH_4NbWO_6 exhibits a 5.8% increase in the cubic unit cell edge once the pressure exceeds ~3.4 GPa, while the $RbNbWO_6$ unit cell expansion is larger (~7.5%) but less abrupt, beginning near 3.0 GPa. Rietveld refinements reveal that the reversible expansion is driven by insertion of water into the structural channels that interpenetrate the $NbWO_6^-$ octahedral corner sharing framework. The insertion of extra water is accompanied by displacement of the NH_4^+ or Rb^+ ions to a smaller site in the channel structure, which triggers the pressure-induced expansion of the pyrochlore framework. This mechanism explains the counterintuitive expansion of the pyrochlore framework in response to application of external pressure. It should be noted that the expansion exhibited by the pyrochlore framework must coincide with a decrease in the volume of the hydrostatic fluid so that the net volume of the system decreases with increasing pressure. Similar behavior is not observed for $KNbWO_6{\cdot}H_2O$ or $HNbWO_6{\cdot}H_2O$, both of which contract in response to increasing pressure. For these smaller monovalent cations, pressure-induced volume expansion does not occur because the hydrated state and subsequent cation shift are already stable at ambient conditions.

Introduction

The phenomenon of pressure-induced volume expansion in materials with open frameworks has received significant attention recently, due in large part to its counterintuitive nature. This property was first observed by Belitsky[1] in the zeolite natrolite. The unit cell volume was shown to increase significantly in water-containing media at about 1 GPa, whereas the volume decreased as expected when other hydrostatic media were used. They suggested that the "anisotropic swelling" observed in natrolite results from the insertion of additional water molecules into its partially filled channels. More recently, the mechanism of this pressure-induced swelling was extensively examined through the use of synchrotron X-ray diffraction and Rietveld refinement in the natrolite family.[2] The volume expansion in natrolite was confirmed to result from the aforementioned selective uptake of water from the hydrostatic fluid into the zeolite framework to form water nanotube-like structures. Additionally, similar pressure-induced volume swelling was observed for three other natrolite topologies: scolecite, mesolite, and a potassium gallosilicate analogue.

It is not only counterintuitive for a material to expand in response to increasing pressure, thermodynamics demands that the total volume of the mixture inside the pressure cell must decrease as the pressure increases. Therefore, pressure-induced expansion of a material will be accompanied by a change in its composition, such as insertion of a species from the pressure-transmitting medium. An extension of this logic suggests that a pressure-induced compositional change is most likely to occur in structures that have cavities, channels, and/or layers where easily exchangeable species (i.e. ions, solvent molecules, etc.) reside. Zeolites and other microporous solids are utilized for their ability to change their composition in response to changes in their environment (as ion-exchange media, molecular sieves, etc.); therefore, in hindsight, it is possible to rationalize the occurrence of pressure-induced swelling in the natrolite family. However, not all framework structures exhibit pressure-induced volume expansion and our understanding of this phenomenon is not sufficient to predict when it will occur. To gain that level of understanding, further mechanistic studies are needed.

[†] The Ohio State University.
[‡] Brookhaven National Laboratory.
[§] University of Birmingham.

(1) Belitsky, I. A.; Fursenko, B. A.; Gabuda, S. P.; Kholdeev, O. V.; Seryotkin, Yu. V. *Phys. Chem. Miner.* **1992**, *18*, 497−505.
(2) Lee, Y.; Vogt, T.; Hriljac, J. A.; Parise, J. B.; Artioli, G. *J. Am. Chem. Soc.* **2002**, *124*, 5466−5475.

10.1021/ja0292187 CCC: $25.00 **© 2003 American Chemical Society**

There is no reason framework structures other than zeolites could not undergo pressure-induced expansion as well, but few examples have been found. One such example is the defect pyrochlore family of compounds. Previously, defect pyrochlores have been studied extensively for potential use as fast ion conductors, due to the high concentration of vacancies within the structure.[3−8] Thus, one would expect reasonably high ion diffusion rates within the rigid octahedral framework, which would seem to be an important characteristic of compounds that undergo pressure-induced expansion. Perottoni and da Jornada noted this feature of the defect pyrochlore structure, leading them to examine the response of NH_4NbWO_6 to high pressures.[9] Through a series of high-pressure energy-dispersive X-ray diffraction experiments they observed a substantial volume increase (∼5%) starting near 2.5 GPa. Furthermore, this expansion was only observed when water was present in the pressure-transmitting hydrostatic medium. They concluded that this behavior is due to insertion of water molecules into the channels of the $NbWO_6^-$ framework. Using computational methods and powder diffraction simulation, it was concluded that the probable site for inserted H_2O in the crystal structure of NH_4NbWO_6 was at the 16e site ($^5/_8$, $^5/_8$, $^5/_8$) of the $F\bar{4}3m$ space group. Additionally, they estimated approximately 0.4 equivalents of water was contained within the high-pressure form of this compound. Even though this study established the existence of pressure-induced volume expansion in ammonium niobium tungstate, several questions regarding the mechanism and generality of this process were left unanswered. For example, since there are natural vacancies in the open channel structure of the defect pyrochlore, why is it necessary for the framework to expand in order to incorporate additional water? Is this behavior general to all defect pyrochlores or limited to NH_4NbWO_6? Does hydrogen bonding play a role, or is the behavior dictated simply by ionic radius considerations? In an attempt to address these questions, we examined the effect of pressure on four different defect pyrochlores, $ANbWO_6$ ($A = NH_4^+$, Rb^+, H^+, K^+), using monochromatic medium-resolution synchrotron X-ray powder diffraction.

Experimental Section

Polycrystalline samples of $KNbWO_6{\cdot}H_2O$[10] and $RbNbWO_6$[11] were prepared by conventional solid-state methods. Stoichiometric amounts of Nb_2O_5 (Alfa, 99.9+% purity) and WO_3 (Aldrich, 99.995% purity) and a 10% excess of Rb_2CO_3 (Cerac, 99.9% purity) or K_2CO_3 (Aldrich, 99.999% purity) were weighed and mixed intimately using acetone in an agate mortar and pestle. Rubidium carbonate and potassium carbonate were used in excess, due to the hygroscopic nature of these reagents and their potential volatility at elevated temperatures. The reaction mixtures were heated in high-form alumina crucibles at 850 °C for 48 h.

NH_4NbWO_6 and $HNbWO_6{\cdot}H_2O$ were prepared from $RbNbWO_6$ and $KNbWO_6{\cdot}H_2O$ by ion exchange methods. NH_4NbWO_6 was synthesized by thoroughly mixing $RbNbWO_6$ with a 20-fold excess of NH_4NO_3 (Fischer, ∼99% purity) in an agate mortar and pestle. The mixture was placed in a high-form alumina crucible and heated between 210 and 220 °C for a total of 20 days.[12] The synthesis of $HNbWO_6{\cdot}H_2O$ was accomplished by heating $KNbWO_6{\cdot}H_2O$ between 55 and 70 °C in 3 M HNO_3 for 20 days.[13] After each heating cycle, the excess ion exchange reagent was separated from the sample by filtration.

All products were analyzed using X-ray powder diffraction (XRPD), infrared spectroscopy (IR), and thermogravimetric analysis (TGA). In-house XRPD was done on a Bruker D8 Advance diffractometer equipped with an incident beam Ge monochromator and a Braun linear position sensitive detector. Rietveld refinement of these data confirmed the formation and purity of the rubidium and potassium compounds and indicated the ion exchange reactions were successful.

IR spectra were collected on samples of each compound in pressed KBr pellets over the range of 500−4000 cm^{-1} using a Mattson Cygnus 100 FTIR. NH_4NbWO_6 was the only compound of the four to show a strong signal at 1414 cm^{-1}, indicative of N−H bond stretches,[14] suggesting that the NH_4^+ for Rb^+ ion exchange was successful. $HNbWO_6{\cdot}H_2O$ and $KNbWO_6{\cdot}H_2O$ spectra looked similar, both showing signals due to water at about 1650 and 3500 cm^{-1}.

TGA was performed on all compounds using a Perkin-Elmer TG 7. The decompositional weight decrease for NH_4NbWO_6 and $HNbWO_6{\cdot}H_2O$, corresponding to the loss of NH_3 and/or H_2O,[15] were 6.82% and 6.90%, respectively, agreeing well with the expected values (6.60% and 6.89%), confirming the expected stoichiometry. Deviation from the ideal weight loss value in NH_4NbWO_6 is attributed to a small amount of water either trapped in the powder and/or adsorbed on the surface. This is further confirmed by the observation of bands at approximately 1650 and 3500 cm^{-1} in the IR spectrum of NH_4NbWO_6. Defect pyrochlores are known to absorb moisture;[3] therefore, the additional weight lost by the ammonium pyrochlore is not surprising. TGA performed on $RbNbWO_6$ and $KNbWO_6{\cdot}H_2O$ showed weight losses of 0.63% and 4.07%, respectively. The theoretical weight loss for the fully hydrated rubidium and potassium compounds ($ANbWO_6{\cdot}H_2O$) correspond to 3.78% and 4.19%. The experimentally determined weight loss shows that $RbNbWO_6$ has very little water of hydration, whereas $KNbWO_6$ is fully hydrated. $KNbWO_6$ is known to easily hydrate in air at room temperature,[16] whereas $RbNbWO_6$ does not hydrate extensively under these conditions.

Medium-resolution ($\Delta d/d \approx 10^{-3}$) XRPD data were collected on each of the pyrochlores on the X7A powder diffractometer at the National Synchrotron Light Source, Brookhaven National Laboratory. Ambient-pressure data were collected on samples sealed in 0.3 mm diameter glass capillaries. Each sample was mounted on a gonioimeter, aligned on the diffractometer, and rocked back and forth for the duration of the collection to reduce the preferred orientation of the crystallites. Data were collected at a wavelength of 0.6942(1) Å over a range of 3−52° 2θ using a position-sensitive detector.[17]

High-pressure powder diffraction data were also collected on the X7A beamline using a focused monochromatic X-ray beam and diamond anvil cell (DAC) following the procedure outlined by Lee.[2] The sample, a few small ruby chips, and the pressure-transmitting fluid (methanol−ethanol−water in a 16:3:1 ratio) were placed in the hole (diameter ∼200−350 μm) of a stainless steel gasket. The gasket was placed between the mounted parallel faces of the diamonds, and the pressure was increased mechanically. Pressure exerted on the sample was measured by detecting the shift in the R1 emission line of the

(3) Goodenough, J. B.; Hong, H. Y−P.; Kafalas, J. A. *Mater. Res. Bull.* **1976**, *11*, 203−220.
(4) Butler, M. A.; Biefeld, R. M. *Solid State Commun.* **1979**, *29*, 5−7.
(5) Bhat, S. V.; Binesh, N.; Bhat, V. *Chem. Phys. Lett.* **1994**, *231*, 487−490.
(6) Hinrichs, R.; Tomandl, G.; da Jornada, J. A. H. *Solid State Ionics* **1995**, *77*, 257−262.
(7) Binesh, N.; Bhat, V.; Bhat, S. V. *Solid State Ionics* **1996**, *86−88*, 665−668.
(8) Hinrichs, R.; Tomandl, G. *Solid State Ionics* **1998**, *107*, 117−122.
(9) Perottoni, C. A.; da Jornada, J. A. H. *Phys. Rev. Lett.* **1997**, *78*, 2991−2994.
(10) Kar, T.; Choudhary, R. N. P. *J. Phys. Chem. Solids* **2001**, *62*, 1149−1161.
(11) Spect, R. W.; Brunner, D. G.; Tomandl, G. *Adv. Ceram. Mater.* **1987**, *2*, 789−93.
(12) Brunner, D. G.; Tomandl, G. *Adv. Ceram. Mater.* **1987**, *2*, 794−97.
(13) Hervieu, M.; Michel, C.; Raveau, B. *Bull. Soc. Chim. Fr.* **1971**, *11*, 3939−3943.
(14) Colthup, N. B. *J. Opt. Soc. Am.* **1950**, *40*, 397−400.
(15) Groult, D.; Michel, C.; Raveau, B. *J. Inorg. Nucl. Chem.* **1974**, *36*, 61−66.
(16) Murphy, D. W.; Cava, R. J.; Rhyne, K.; Roth, R. S.; Santoro, A.; Zahurak, S. M.; Dye, J. L. *Solid State Ionics* **1986**, *18−19*, 799−801.
(17) Smith, G. C. *Synchrotron Radiat. News* **1991**, *4*, 24−30.

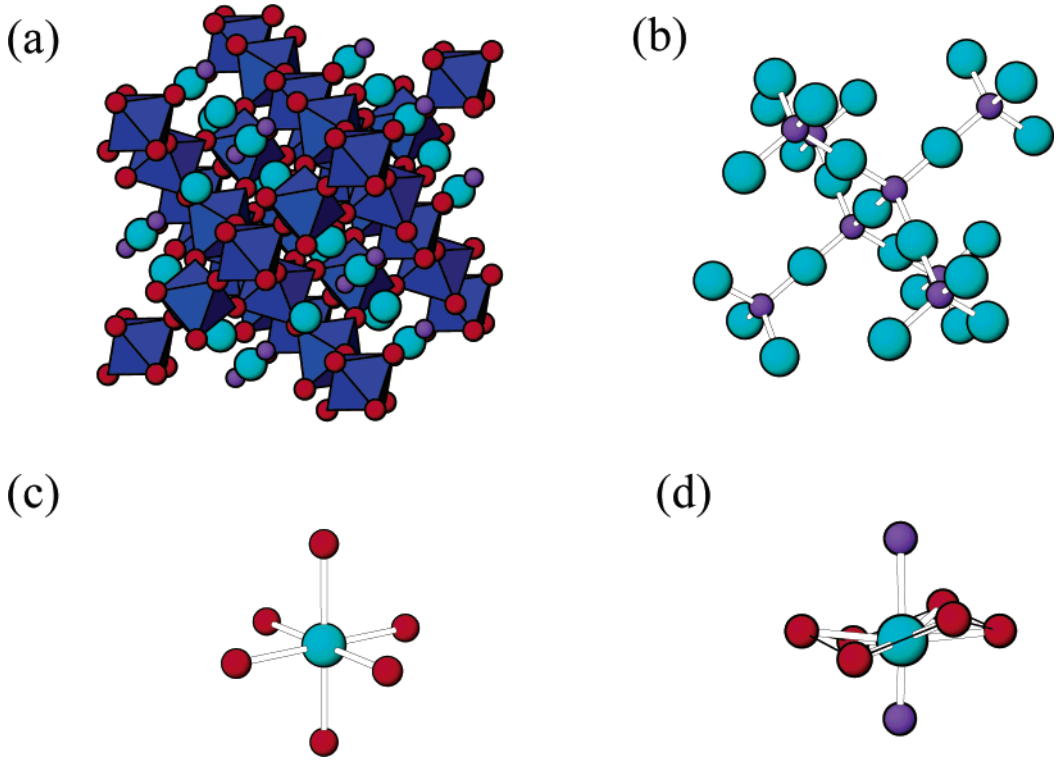

Figure 1. (a) The ideal pyrochlore structure, $A_2M_2X_6X'$. Colors representing the ions in the structures are as follows: A, cyan; M, dark blue; X, red; X′, violet. (b) Anticristobalite-like A_2X' network in the ideal pyrochlore. (c) Coordination of rubidium in the defect pyrochlore $RbNbWO_6$. Rb^+ fully occupies the 8b site ($^3/_8$, $^3/_8$, $^3/_8$) and is octahedrally coordinated to lattice oxygen (6 Rb−O bonds 3.254(5) Å). (d) Coordination of K in $KNbWO_6{\cdot}H_2O$. K^+ partially occupies ($^1/_4$) the 32e site (x, x, x; $x \approx 0.49$) and lies near the middle of a ring of six lattice oxygens arranged in a manner similar to the chair configuration of cyclohexane. If water is present (shown in violet), K^+ is eight-coordinate with six equatorial lattice oxygens (K−O bond lengths 2.724(5) Å (×3), 2.786(7) Å (×3)) and axial coordination by water molecules (K−OH_2 distances 2.28(2), 2.86(1) Å).

included ruby chips,[18] and the instrumental errors on the pressure measurements ranged between 0.05 and 0.10 GPa. It should be noted that, during the data collection, all four pyrochlores, initially white, turned violet when irradiated. XRPD data were collected in multiple trials from 3 to 35° 2θ (0.25° steps, 60−180 s/step) at a wavelength of ~0.7 Å for pressures up to 7 GPa.

XRPD data were analyzed using the EXP-GUI version of the GSAS Rietveld package.[19,20] The bent Si (220) monochromator, necessary for focusing, diffracts a small amount of $\lambda/2$ radiation (1−2% of the intensity of the primary radiation). These $\lambda/2$ peaks were accounted for in the data treatment. Regions of the diffraction pattern exhibiting reflections due to the presence of the gasket or ruby chip were excluded. Despite the observation of narrow ruby fluorescence peaks, some runs produced XRPD patterns that exhibited a relatively minor, noninstrumental, asymmetry in the peak shape. In some cases this was accompanied by the observation of phase separation at high pressures. We suspect these effects are due to either compositional/pressure gradients or slight nonhydrostaticity. After several loadings of the NH_4^+ and Rb^+ samples, data suitable for Rietveld analyses were obtained, whereas we were not able to completely eliminate noninstrumental peak-broadening effects for the K^+ and H^+ samples. For these compounds model-based LeBail fitting[19−21] was performed in order to extract the evolution of the cubic unit cell edge, but full Rietveld refinements were not attempted. In all cases, there was little change in the background as a function of pressure, suggesting pressure-induced amorphization did not occur. On the basis of this observation, we have assumed the sample retains 100% crystallinity in all refinements. Finally, bulk moduli (K_o) were determined for each compound by fitting the Birch−Murnaghan equation of state (EOS) to the normalized volumes ($V/V_o = [1 + K'P/K_o]^{-1/K'}$), with $K' = 4$ using EOSFIT, version 6.0.[22]

Results and Discussion

Ambient-Pressure Structures. The ideal pyrochlore structure has cubic symmetry (space group $Fd\bar{3}m$), as depicted in Figure 1. Its stoichiometry is $A_2M_2X_6X'$, where A is a large, low-oxidation-state cation (i.e. a lanthanide, alkali-metal, or alkaline-earth-metal cation) and M is a smaller cation that can adopt octahedral coordination (i.e. Ti^{4+}, Zr^{4+}, Ru^{4+}, Sn^{4+}); X is typically oxygen, while X′ is also an anion (i.e. O^{2-}, F^-, OH^-). The A-site ions reside on the 16d Wyckoff site, the M-site ions on the 16c Wyckoff site, the X ions on a 48f site, and the X′ ions on the 8b site. The structure can be described as two interpenetrating networks. The MX_6 octahedra share corners to form a three-dimensional M_2X_6 framework, within which a 3D labyrinth of channels exists. The A_2X' network forms an anti-cristobalite network that fills the empty channels of the M_2X_6 framework. The two networks are linked through the interaction between the large cations, A, and the framework oxygens, X. This leads to 8-fold coordination for the A-site cations ($AX_6X'_2$).[23] The defect AM_2X_6 pyrochlore structure can be derived from

(18) Piermarini, G. J.; Block, S.; Barnett, J. D. *J. Appl. Phys.* **1973**, *44*, 5377−5382.
(19) Larson, A. C.; von Dreele, R. B. *GSAS: General Structure Analysis System*; Los Alamos National Laboratory Report LAUR 86-748; Los Alamos National Laboratory: Los Alamos, NM, 2000.
(20) Toby, B. H. *J. Appl. Crystallogr.* **2001**, *34*, 210−213.
(21) LeBail, A.; Duroy, H.; Fourquet, J. L. *Mater. Res. Bull.* **1988**, *23*, 447−452.
(22) Angel, R. J. Equations of State. In *High-Temperature and High-Pressure Crystal Chemistry*; Hazen, R. M., Downs, R. T., Eds.; The Mineralogical Society of America: Washington, DC, 2000; Vol. 41, pp 35−58.
(23) Sleight, A. W. *Inorg. Chem.* **1968**, *7*, 1704−1708.

Table 1. Rietveld Refinement Details for $ANbWO_6$ at Ambient Pressures[a]

	NH_4NbWO_6	$HNbWO_6{\cdot}H_2O$	$KNbWO_6{\cdot}H_2O$	$RbNbWO_6$
		Crystal Data		
space group, Z	$F\bar{4}3m$, 8[b]	$Fd\bar{3}m$, 8[c]	$Fd\bar{3}m$, 8[c]	$Fd\bar{3}m$, 8[c]
a (Å)	10.3792(1)	10.4134(1)	10.5073(1)	10.3736(1)
R_p (%)	3.60	3.11	5.46	4.59
R_{wp} (%)	4.70	4.89	7.22	6.49
χ^2	3.97	25.88[d]	5.62	7.42
		Atomic Positions		
Nb/W				
site	16e	16c	16c	16c
x	0.12979(6)	0	0	0
U_{iso}		2.15(2)	2.06(3)	2.38(4)
U_{11}[e]	1.73(2)			
U_{12}[e]	−1.72(2)			
A(1)				
type	N (NH_4^+)	O (H_3O^+)	K	Rb
site	16e	32e	32e	8b
x	0.510(9)	0.349(7)	0.4838(6)	$^3/_8$
U_{iso}	3.2(7)	5.2(15)	0.5(3)	7.0(2)
occupancy	0.25	0.25	0.25	1
A(2)				
type	N (NH_4^+)			
site	16e			
x	0.787(4)			
U_{iso}	3.2(7)			
occupancy	0.25			
O(1)				
site	24f	48f	48f	48f
x	0.182(1)	0.3072(4)	0.3064(6)	0.3116(6)
U_{iso}	0.6(1)	0.7(1)	1.5(2)	0.9(2)
O(2)				
site	24g	24g	32e	
x	0.447(1)		0.412(1)	
U_{iso}	0.6(1)		1.7(10)	
occupancy			0.25	
		Selected Bond Lengths (Å)		
Nb/W−O(1)	3 × 1.988(3)	6 × 1.933(1)	6 × 1.950(2)	6 × 1.941(1)
Nb/W−O(2)	3 × 1.938(4)			
A−O(1)			3 × 2.733(5)	6 × 3.254(3)
			3 × 2.806(5)	
A−O(2)			1 × 2.29(2)	
			1 × 2.86(1)	

[a] Esd's are given in parentheses. All sites are fully occupied unless explicitly noted in the table. [b] Wyckoff positions and occupancies for space group $F\bar{4}3m$: 16e site (x, x, x); 24f site (x, 0, 0); 24g site (x, $^1/_4$, $^1/_4$). [c] Wyckoff positions and occupancies for space group $Fd\bar{3}m$: 16c site (0, 0, 0); 8b site ($^3/_8$, $^3/_8$, $^3/_8$); 32e site (x, x, x); 48f site (x, $^1/_8$, $^1/_8$). Note the reported O(2) for $KNbWO_6{\cdot}H_2O$ corresponds to H_2O occupying a 32e site. [d] The high χ^2 value reported for $HNbWO_6{\cdot}H_2O$ is a consequence of having a flat, low-noise background; therefore, the fit of the data was not as good as the refinement program expected. [e] Anisotropic displacement parameters were used for Nb and W; $U_{11} = U_{22} = U_{33}$ and $U_{12} = U_{13} = U_{23}$ in NH_4NbWO_6. The reasoning behind using anisotropic displacement parameters for the refinement of NH_4NbWO_6 is described elsewhere.[25] All displacement parameters are given in units of Å^2 (×100).

the ideal structure by removing 50% of the cations and 100% of the anions from the A_2X' network.[24] There are three possible locations for the A-cation: (a) on the 8b site (fully occupied), (b) on the 16d site (50% occupancy), (c) or on an intermediate position, which can be modeled using a partially occupied 32e site.

Numerical details of the refined ambient-pressure models for all four compounds are given in Table 1. For NH_4NbWO_6,[25] $RbNbWO_6$,[26,27] and $KNbWO_6{\cdot}H_2O$,[16] these agree well with previous reports. Structural data were not found in the literature for $HNbWO_6{\cdot}H_2O$; therefore, its structure was refined using the structure of $HTaWO_6{\cdot}H_2O$[28] as a starting model for the refinement. NH_4NbWO_6 was refined using the noncentrosymmetric space group $F\bar{4}3m$.[25] The refined positions of the A-site cations (16e, x, x, x; A(1) $x \approx {}^1/_2$, A(2) $x \approx {}^3/_4$) are closely related to the 8b site ($^3/_8$, $^3/_8$, $^3/_8$) within the centrosymmetric space group $Fd\bar{3}m$. The M-site cations were assumed to be completely disordered in all four compounds, and no evidence was found to dispute this.

$RbNbWO_6$ was refined using the centrosymmetric space group $Fd\bar{3}m$ as previously reported.[26,27] A subtle tetragonal distortion has been reported in $RbNbWO_6$ ($c/a = 1.0018$),[29] but an appropriate space group has never been determined for this compound, and we did not observe any peak splitting indicative of noncubic symmetry. Note that Rb fully occupies the 8b site at ambient pressures; its coordination is shown in Figure 1c.

$KNbWO_6{\cdot}H_2O$ was refined in a manner identical with that for $RbNbWO_6$. It has been previously reported that $KNbWO_6$ exists in both hydrated and nonhydrated forms.[16] It is important to point out that K^+ resides on a 32e site in both forms, but its position differs significantly between the two compositions. In $KNbWO_6$, the potassium ions are located close (0.4086, 0.4086, 0.4086) to the 8b site ($^3/_8$, $^3/_8$, $^3/_8$), whereas in $KNbWO_6{\cdot}0.69\ D_2O$, K^+ sits at (0.4857, 0.4857, 0.4857), very close to the 16d site ($^1/_2$, $^1/_2$, $^1/_2$), and water sits on a 32e site ($x = 0.4143$), once again close to the 8b site. After the lattice parameter was determined ($a = 10.5073(1)$ Å), a model similar to that of $KNbWO_6{\cdot}0.69D_2O$ was used to fit the data. The coordination of K^+ in $KNbWO_6{\cdot}H_2O$ is shown in Figure 1d.

$RbNbWO_6$ at High Pressure. Rietveld refinement results for $RbNbWO_6$ as a function of pressure are summarized in Table 2. We followed the aforementioned precedent by using the centrosymmetric cubic space group $Fd\bar{3}m$ for all refinements.[26,27] The unit cell edge length, as well as positions, occupancies, and displacement parameters of the rubidium ions and water molecules were extracted from the diffraction data. Thermal parameters for the atoms defining the $NbWO_6^-$ framework were allowed to deviate from the values determined from the ambient-pressure refinement. The fractional occupancy of water was refined for the hydrated phase until it reached a value corresponding to one water molecule/formula unit (fractional occupancy $^1/_4$ on water's 32e site; x, x, x). For some of the data sets (pressures of 4.26, 4.67, and 5.15 GPa) the refined water occupancy slightly exceeded 0.25, which is a chemically unreasonable result due to steric hindrance. In these cases the occupancy was fixed at 0.25, and the rest of the aforementioned parameters were refined. The goodness of fit parameters did not change significantly in response to this constraint, suggesting that occupancies greater than 0.25 arise as a consequence of correlations with displacement parameters.

Evolution of the unit cell volume for $RbNbWO_6$ is given in Figure 2b. Similar to the phenomenon previously observed in NH_4NbWO_6, a drastic increase in unit cell volume occurs above

(24) Babel, D.; Pausewang, G.; Viebahn, W. *Z. Anorg. Allg. Chem.* **1972**, *161*, 387.
(25) Perottoni, C. A.; Haines, J.; da Jornada, J. A. H. *J. Solid State Chem.* **1998**, *141*, 537−545.
(26) Bydanov, N. N.; Chernaya, T. S.; Muradyan, L. A.; Sarin, V. A.; Rider, E. E.; Yanovskii, V. K.; Bosenko, A. A. *Kristallografiya* **1987**, *32*, 623−630.
(27) Chernaya, T. S.; Bydanov, N. N.; Muradyan, L. A.; Savan, V. A.; Simonov, V. I. *Kristallografiya* **1988**, *33*, 75−81.
(28) Groult, D.; Pannetier, J.; Raveau, B. *J. Solid State Chem.* **1982**, *41*, 277−285.
(29) Sleight, A. W.; Zumsteg, F. C.; Barkley, J. R.; Gulley, J. E. *Mater. Res. Bull.* **1978**, *13*, 1247−1250.

Table 2. Refined Lattice Parameters, Phase Fractions, and Atomic Parameters for $RbNbWO_6$ at Different Pressures[a]

	pressure (GPa)[b]								
	0.62(↑)	2.12(↑)	2.79(↑)	3.47(↑)	3.99(↑)	4.67(↑)[c]	5.15(↑)[c]	4.26(↓)	0.99(↓)
R_p (%)	5.10	5.19	3.93	3.85	4.94	4.77	3.82	3.56	4.00
R_{wp} (%)	6.93	6.65	5.36	5.32	6.39	6.54	5.13	4.50	5.12
χ^2	5.63	4.51	4.05	4.30	5.11	7.08	4.54	3.14	3.62
				Phase 1					
a (Å)	10.3544(2)	10.3034(1)	10.2810(1)	10.2632(1)	10.2449(4)	10.2081(7)	10.177 (1)	10.2724(2)	10.3572(1)
mass fraction (%)	100	100	100	98.5(5)	88.2(1)	37.2(4)	6.9(4)	28.8(2)	100
				Phase 2					
a (Å)				10.522(1)	10.4868(4)	10.4808(2)	10.4676(1)	10.4967(1)	
mass fraction (%)				1.5(5)	11.8(2)	58.0 (2)	90.8 (5)	71.2 (1)	
Rb position[d]				0.481[e]	0.481[e]	0.481 (2)	0.481 (1)	0.480(1)	
H_2O position[d]				0.420[e]	0.420[e]	0.416 (2)	0.420 (2)	0.411 (1)	
				Bond Lengths (Å)[f]					
Nb/W−O (×6)	1.926(2)	1.932(2)	1.932(1)	1.929(2)	1.905(5)	1.951(4)	1.963(2)	1.957(2)	1.940(2)
Rb−O	6 × 3.283(7)	6 × 3.219(6)	6 × 3.201(1)	6 × 3.193(5)	6 × 3.25(2)	3 × 2.799(7)	3 × 2.744(9)	3 × 2.799(7)	6 × 3.243(5)
						3 × 2.714(9)	3 × 2.672(5)	3 × 2.706(5)	
Rb−H_2O						1 × 2.95(4)	1 × 2.98(2)	1 × 2.92(2)	
						1 × 2.29(5)	1 × 2.33(3)	1 × 2.23(3)	

[a] Esd's are given in parentheses. Errors for the reported pressures ranged between 0.05 and 0.10 GPa. [b] Legend: ↑, data collected upon increasing pressure; ↓, data collected upon decreasing pressure. [c] A smaller, third cubic phase of unknown origin is seen in these diffraction patterns; at 4.67 GPa, a=10.131(1) Å with a mass fraction of 4.8(2)%; at 5.15 GPa, a=10.012(3) Å with a mass fraction of 2.3(1)%. [d] Wyckoff positions for selected phase 2 atoms: Rb 32e site (x, x, x; occupancy = 0.25); H_2O 32e site (x, x, x). The water site occupancy was set at 0.25. [e] Atomic positions for Rb^+ and H_2O fixed at values determined at 5.15 GPa. Atomic positions could not be refined adequately due to the small phase fraction of the hydrated phase. [f] Bond lengths given for majority phase only. All data sets were refined using the space group $Fd\bar{3}m$. Atomic positions, thermal parameters, lattice parameters, and profile coefficients were refined for each data set.

3 GPa. However, as shown in Figure 2a, diffraction patterns with pressures ≥3.47 GPa show two cubic phases,[30] one having a significantly larger unit cell volume than the ambient pressure value. The unit cell volume observed for the majority phase in $RbNbWO_6$ at 4.67 GPa (mass fraction 58.0(2)%) is 3.1(1)% greater than its value at ambient pressure and 7.5(1)% greater than the value extrapolated from the lower pressure data. The volume expansion observed here is larger than but not as abrupt as that observed in NH_4NbWO_6. The fraction of the hydrated (larger volume) phase increases between 3.47 and 5.72 GPa, reaching a maximum of 90.8(5)%. Difference Fourier mapping, powder pattern simulation, and finally Rietveld refinements leave no doubt that the water insertion is accompanied by the movement of rubidium cations in the channels. As shown in Figure 2c, rubidium moves from its ambient-pressure position on the 8b site ($^3/_8$, $^3/_8$, $^3/_8$) to a 32e position very close to the 16d site (where the A-cation normally resides in a stoichiometric pyrochlore). The refinements reveal water molecules also residing in the channels on a 32e site ($x \cong 0.42$) at 4.67 GPa. The refined positions of Rb and H_2O in the hydrated form are almost identical with those of potassium and water in $KNbWO_6 \cdot H_2O$ at ambient pressure, showing $RbNbWO_6$ adopts a high-pressure form isostructural with the ambient-pressure form of its potassium counterpart.

These results allow us to construct a picture of the mechanism that drives the pressure-induced volume expansion. The Rb^+ shift occurs in order to make room for water to be inserted into the channels. However, the shift also drives Rb^+ to a coordination environment where the Rb−O bonds are considerably shorter than would normally be observed under ambient conditions (see Table 2). To alleviate the tight fit of the Rb^+ ions, the octahedral framework is forced to expand, giving rise to an increase in the unit cell volume. It is likely that the oxygen ions in the vicinity of the rubidium ion relax somewhat as well, but we are not able to extract enough detail from the refinements to comment definitively on this point. As the pressure is released, deinsertion of water and the subsequent shift of rubidium back to the 8b site occurs. It would be interesting to compare the abrupt contraction of the rubidium coordination environment with the behavior of other rubidium-containing compounds. Unfortunately, we were unable to find any reports of Rb−O compressibility studies in the literature. Nonetheless, one would expect that the long, highly ionic Rb−O bonds would be highly compressible.

NH_4NbWO_6 at High Pressure. Rietveld refinement results for NH_4NbWO_6 as a function of pressure are summarized in Table 3. Refinements based on the noncentrosymmetric $F\bar{4}3m$ space group were problematic, because in the DAC, very weak reflections specifically associated with $F\bar{4}3m$ symmetry are indistinguishable from the background noise. Naturally this leads to unwanted correlations between NH_4^+ and H_2O positional parameters when using the $F\bar{4}3m$ model, not to mention the possibility that the application of pressure may in fact stabilize the centrosymmetric $Fd\bar{3}m$ symmetry. Therefore, we elected to analyze the data using the centrosymmetric space group $Fd\bar{3}m$, in a manner identical with that used for $RbNbWO_6$. While this approach may be an approximation to the exact crystal structure, it is sufficiently accurate to extract the important details regarding the mechanism of the pressure-induced volume expansion.

A small region of each NH_4NbWO_6 diffraction pattern is shown in Figure 3a. Note that below 1.97 GPa the peak positions shift to higher angles as the pressure increases, indicating a contraction of the unit cell. Between 1.97 and 3.37 GPa, one observes a dramatic shift of the peak positions to lower angles, corresponding to an increase in unit cell volume. A plot of the

(30) We also noted a very small amount of a third phase at 4.67 and 5.15 GPa. Its lattice parameter is significantly smaller than either of the other two phases, and its mass fraction (based on the low-pressure crystal structure of $RbNbWO_6$) is less than 5%. The minute concentration of this phase prevented determination of any parameters other than the unit cell edge and mass fraction. At this time, its origin is unclear.

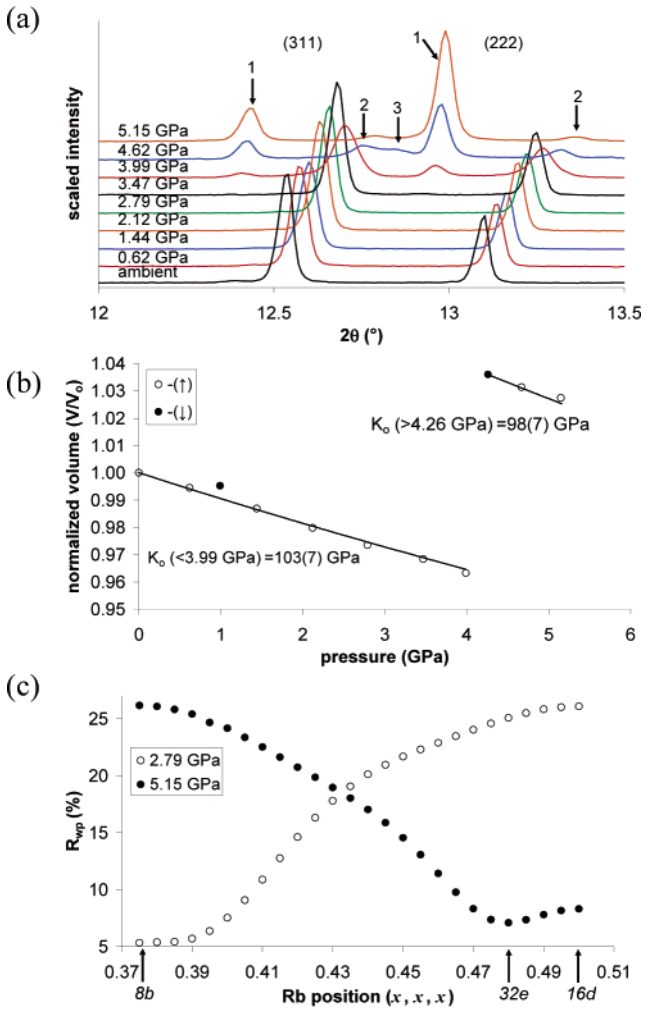

Figure 2. (a) Partial powder diffraction patterns of $RbNbWO_6$ (DAC loading #2) at various pressures. Note the formation of at least two phases at pressures greater than 3.99 GPa. Reflections marked with "1" correspond to the hydrated phase, and those marked with "2" are related to the original compound. The peak marked "3" corresponds to the strongest reflection of a third cubic phase (origin and composition unknown). (b) Evolution of the unit cell volume of $RbNbWO_6$ (DAC loading #2), normalized with the ambient pressure value. Data for a trial collected with increasing pressure is marked with ↑. Data for a trial collected as the applied pressure was released is marked with ↓. At pressures ≥3.47 GPa, V/V_o is given for the majority phase only. Esd's for the normalized volumes are not included, because their span is less than the width of the data points. Errors for the reported pressures ranged between 0.05 and 0.10 GPa and are not included on the figure. Bulk moduli (K_o) were calculated by fitting the Birch−Murnaghan EOS (shown in the figure) to the normalized volumes, where $K' = 4$. (c) The change in goodness of fit parameter, R_{wp}, as a function of Rb^+ position in the unit cell at 2.79 and 5.15 GPa. The 32e site marked with an arrow corresponds to (0.48, 0.48, 0.48).

unit cell volume evolution for all trials is given in Figure 3b. Below 1.97 GPa, the unit cell volume of the nonhydrated compound compresses regularly. At 3.37 GPa, the compound's unit cell volume expands abruptly. At its maximum (3.37 GPa) it is 3.3(1)% larger than its volume at ambient pressure and 5.8(1)% larger than the expected unit cell volume, on the basis of extrapolation of the data collected below 2 GPa. Further increases in pressure lead to further contraction of the unit cell volume. This behavior agrees with the earlier work of Perottoni and da Jornada.[9]

Data were also collected upon releasing pressure, which differed somewhat from the previous study. As shown in Figure 3a, two distinct phases were observed as the pressure was slowly released (in trial 3). After initially observing two cubic phases at 2.87 GPa, the sample was set aside for 2 h and an additional diffraction pattern was taken without adjusting the pressure. The pressure, taken after XRPD data were collected, had dropped to 2.59 GPa, and the mass fraction of the less hydrated (smaller volume) phase was observed to increase. As the pressure was further decreased mechanically, the mass fraction of the less hydrated phase continued to increase while the mass fraction of the more hydrated (larger volume) phase slowly decreased (see Table 3). After the pressure dropped below 2 GPa, a single phase was observed, but the unit cell volume still remained slightly larger than was observed upon increasing pressure. This behavior shows that the kinetics of the pressure-induced water insertion and the corresponding deinsertion reaction are relatively slow. Furthermore, it appears as though some water is retained by the pyrochlore framework as the pressure is released. This is reflected in the lattice parameter and crystallographic positions of NH_4^+ and H_2O at 2.07 and 2.33 GPa.

It was previously suggested that the inserted water molecules reside in the vicinity of the stoichiometric pyrochlore A site ($F\bar{4}3m$, Wyckoff site 16e at x, x, x, where $x \approx {}^5/_8$; equivalent to the 16d site in $Fd\bar{3}m$, ${}^1/_2, {}^1/_2, {}^1/_2$), while the ammonium cations stay in the vicinity of the X′ site ($F\bar{4}3m$, Wyckoff site 16e, where $x \approx {}^1/_2$ and ${}^3/_4$; equivalent to the 8b site in $Fd\bar{3}m$, ${}^3/_8, {}^3/_8, {}^3/_8$).[9] Our Rietveld refinements do not directly contradict this conclusion, in that we find either NH_4^+ or H_2O residing on two distinct 32e sites (x, x, x), one with $x \approx 0.49$ and the other with $x \approx 0.42$. However, using XRPD, it is not possible to accurately distinguish between ammonium cations and water molecules. Therefore, we can only comment on the total occupancies of the A and X′ sites. It is very instructive to note that these values correspond quite closely with the refined positions of Rb^+ (32e site with $x \approx 0.48$) and H_2O (32e site with $x \approx 0.42$) in $RbNbWO_6$. On the basis of the similarities in crystal structure and the monovalent ionic radii (NH_4^+ at 1.60−1.75 Å[31,32] and eight-coordinate Rb^+ at 1.75 Å[31]) it appears that the same mechanism (cation migration accompanied by water insertion) can be invoked to explain the pressure-induced volume expansion in both $RbNbWO_6$ and NH_4NbWO_6.

$KNbWO_6 \cdot H_2O$ and $HNbWO_6 \cdot H_2O$ at High Pressure. The evolution of the unit cell volume as a function of pressure is presented in Figures 4 and 5 for $KNbWO_6 \cdot H_2O$ and $HNbWO_6 \cdot H_2O$, respectively. In both cases our attempts at full Rietveld refinements were hampered by the asymmetric peak shapes, characteristic of either nonhydrostatic conditions and/or compositional/pressure gradients. The unit cell volume of $KNbWO_6 \cdot H_2O$ steadily decreases with increasing pressure, in contrast to the behavior seen in the aforementioned compounds. As shown in Figure 4a, the partial diffraction patterns show no significant change in the intensities of any reflections. This suggests that K^+ does not shift significantly from its original position within the unit cell, and very little if any additional water is forced into the structure upon application of pressure. $HNbWO_6 \cdot H_2O$ behaves in a similar fashion, as seen in Figure 5a. Figure 5b shows the evolution of the unit cell volume as a function of pressure for four different DAC loadings of this compound. Interestingly, starting at 3.16 GPa, there is a slight increase in

(31) Shannon, R. D. *Acta Crystallogr.* **1976**, *A32*, 751−767.
(32) Jacobson, A. J.; Johnson, J. W.; Lewandowski, J. T. *Mater. Res. Bull.* **1987**, *22*, 45−51.

Table 3. Refined Lattice Parameters and Phase Fractions for NH_4NbWO_6 at Different Pressures[a]

	pressure (GPa)[b]								
	1.01 (↑)	1.97 (↑)	3.37 (↑)	4.00 (↑)	6.35 (↑)	2.87 (↓)	2.59 (↓)	2.33 (↓)	2.07 (↓)
R_p (%)	4.97	6.11	4.53	4.20	4.20	4.76	4.44	5.32	5.17
R_{wp} (%)	6.65	9.35	6.62	6.30	5.79	6.68	6.50	7.00	6.94
χ^2	3.82	4.64	3.71	5.72	7.14	4.44	5.05	2.19	2.21
				Phase 1					
a (Å)	10.353(2)	10.360(2)				10.418(6)	10.409(4)	10.414(3)	10.414(1)
mass fraction (%)	100	100				9.2(2)	18.0(3)	83.4(1)	94.2(5)
NH_4^+ position[c]	0.375	0.375				0.375	0.375	0.475(4)	0.464(3)
H_2O position[c]								0.404(3)	0.38(1)
				Phase 2					
a (Å)			10.490(1)	10.483(1)	10.419(2)	10.502(2)	10.509(2)	10.531(4)	10.535(1)
mass fraction (%)			100	100	100	90.8(2)	82.0(2)	16.6(2)	5.8(3)
NH_4^+ position[c]			0.484(2)	0.489(2)	0.494(6)	0.487(3)	0.480[d]	0.480[d]	0.480[d]
H_2O position[c]			0.432(2)	0.443(2)	0.438(2)	0.425(3)	0.427(2)	0.427[d]	0.427[d]
				Bond Lengths (Å)[e]					
Nb/W−O (×6)	1.955(3)	1.932(2)	1.988(3)	1.977(2)	1.965(3)	1.984(3)	1.968(3)	1.958(4)	1.961(5)
NH_4^+−O	6 × 3.194(9)	6 × 3.219(6)	3 × 2.631(6)	3 × 2.657(6)	3 × 2.647(9)	3 × 2.649(8)	3 × 2.69(5)	3 × 2.625(9)	3 × 2.65(2)
			3 × 2.72(1)	3 × 2.715(4)	3 × 2.68(3)	3 × 2.722(8)	3 × 2.79(5)	3 × 2.758(9)	3 × 2.84(9)
NH_4^+−H_2O			1 × 3.08(2)	1 × 2.99(3)	1 × 2.95(2)	1 × 2.94(3)	1 × 3.09(3)	1 × 2.92(7)	1 × 2.97(6)
			1 × 2.53(3)	1 × 2.62(4)	1 × 2.75(2)	1 × 2.49(3)	1 × 2.40(2)	1 × 2.17(6)	1 × 2.65(5)

[a] Esd's are given in parentheses. Errors for the reported pressures ranged between 0.05 and 0.10 GPa. [b] Legend: ↑, data collected upon increasing pressure; ↓, data collected upon decreasing pressure. [c] Wyckoff position for NH_4^+/H_2O 16e site (x, x, x; occupancy = 0.25). Water and ammonium positions were refined for data collected at 2.07 GPa (↓) and 2.33 GPa (↓) because the intensities of the reflections suggested that residual water was still present in the crystal structure below the volume expansion threshold pressure. [d] The free positional parameters for NH_4^+ and/or H_2O at $P \geq 2.59$ GPa could not be refined. The value was set at 0.480 for NH_4^+ and 0.427 for H_2O. Bond length calculations for NH_4NbWO_6 at this pressure were determined using the previously mentioned value. [e] Bond lengths given for the majority phase only. All data sets were refined using the space group $Fd\bar{3}m$. Atomic positions, thermal parameters, lattice parameters, and profile coefficients were refined for each data set.

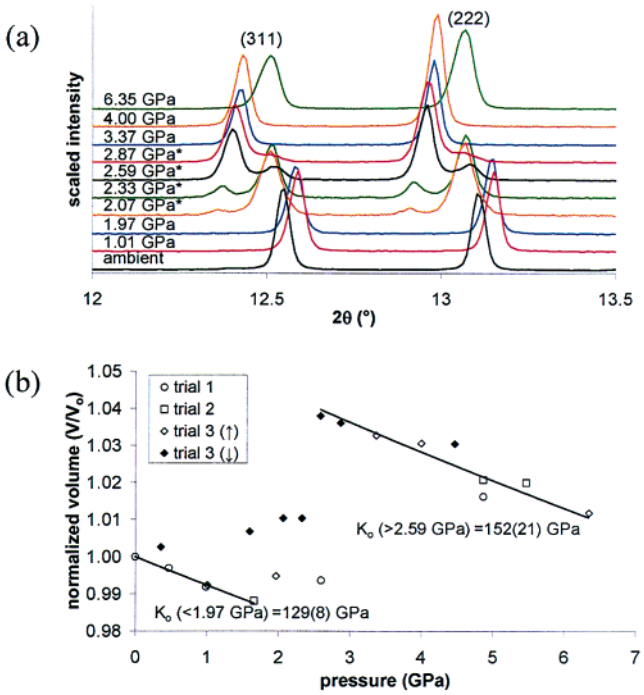

Figure 3. (a) Partial powder diffraction patterns of NH_4NbWO_6 (DAC loading #3) at various pressures. Asterisks denote diffraction data that were collected as the pressure was slowly released. Note the formation of two phases between 2.07 and 2.87 GPa upon pressure release. (b) Evolution of the reduced unit cell volume as a function of pressure in NH_4NbWO_6 (all DAC loadings). The conventions, errors, and bulk moduli fitting utilized in Figure 2b are applied here. Between 2.07 and 2.87 GPa, V/V_o is given for the majority phase only.

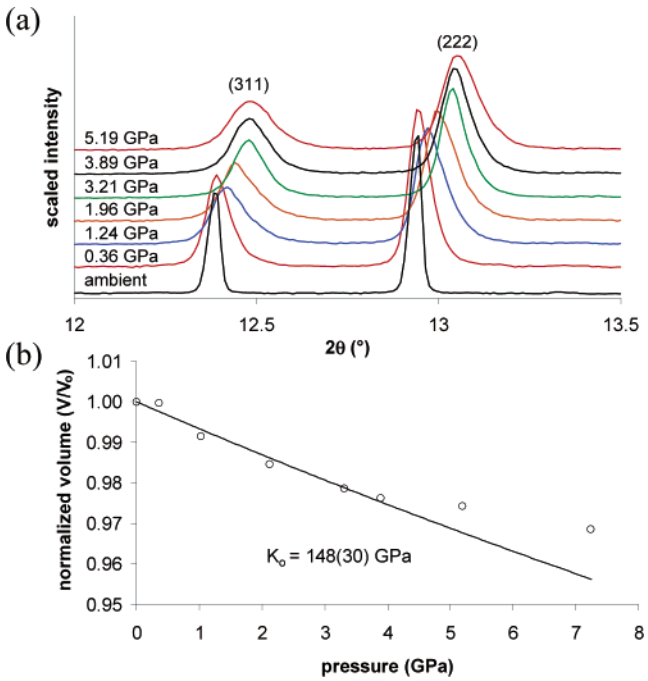

Figure 4. (a) Partial powder diffraction patterns of $KNbWO_6 \cdot H_2O$ (DAC loading #1) at various pressures. (b) Evolution of the reduced unit cell volume as a function of pressure in $KNbWO_6 \cdot H_2O$. The conventions, errors, and bulk moduli fitting utilized in Figure 2b are applied here.

the unit cell volume, followed by a change in the slope of the unit cell volume evolution. Examination of the diffraction patterns (Figure 5a) reveals a small change in the relative intensities of the (311) and (222) reflections, suggesting that some water may be inserted into the unit cell upon increasing pressure. Clearly, the volume increase observed here is considerably smaller than that seen in the rubidium or ammonium compounds and further analysis was not possible.

Conclusion

The strikingly different behaviors exhibited by the four compounds examined in this study can be attributed to differ-

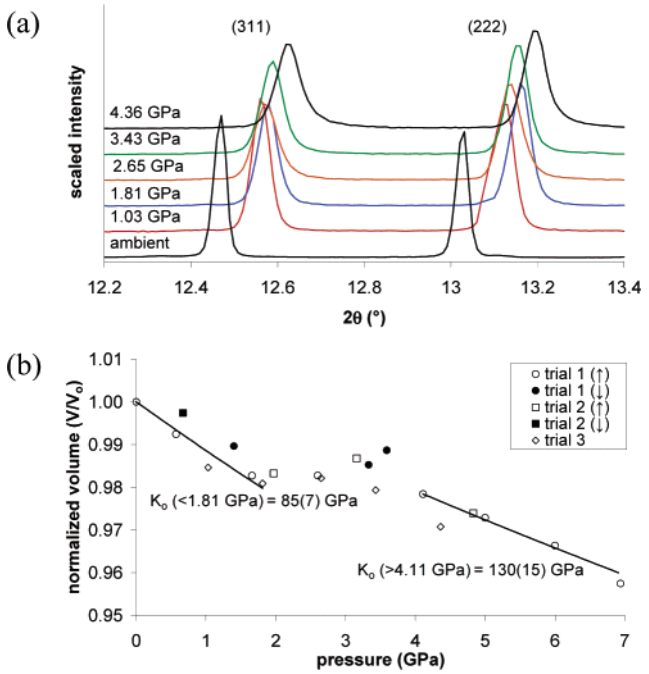

Figure 5. (a) Partial powder diffraction patterns of $HNbWO_6 \cdot H_2O$ (DAC loading #3) at various pressures. (b) Evolution of the reduced unit cell volume as a function of pressure in $HNbWO_6 \cdot H_2O$. The conventions, errors, and bulk moduli fitting utilized in Figure 2b are applied here.

ences in the size of the monovalent cations located in the pyrochlore channels. Rb^+ and NH_4^+ have similar ionic radii, whereas K^+ is considerably smaller.[33] As a result, at ambient pressure the Rb^+ and NH_4^+ ions are too large for the coordination environment close to the 16d site, which is the preferred site for smaller cations including K^+, and must occupy the 8b site. Cation occupation of the 8b site also seems to lead to the exclusion of water from the pyrochlore channels, to a large extent. Upon application of pressure it becomes energetically favorable to shift the large cations from the 8b site to the vicinity of the smaller 32e ($x \cong 0.485$) site while simultaneously incorporating water into the channels. The volume expansion of the $NbWO_6^-$ framework is a response to this cation shift. Similar behavior is not observed in $KNbWO_6 \cdot H_2O$, due to the fact that even at ambient pressure the K^+ ion is already at the 32e site and the compound is partially hydrated. Consequently, there is no driving force to superhydrate this structure. Further evidence for this conclusion comes from the fact that if one dehydrates $KNbWO_6 \cdot H_2O$ at ambient pressure, the potassium shifts back to a position (0.4068, 0.4068, 0.4068) near the 8b site and the unit cell volume contracts from 1160 $Å^3$ to 1113 $Å^3$.[16] Similarly, $H(H_2O)^+$ does not appear to be of adequate size for water insertion to trigger a significant expansion of the $NbWO_6^-$ framework. Unlike in natrolite,[2] it would appear that hydrogen bonding is not a critical component of the pressure-induced volume expansion phenomenon in the defect pyrochlore family.

Of the $ANbWO_6$ pyrochlores investigated here, the $RbNbWO_6$ and NH_4NbWO_6 pyrochlores show *significant and abrupt increases in unit cell volume above* ~3 GPa, whereas $KNbWO_6 \cdot H_2O$ and $HNbWO_6 \cdot H_2O$ show normal compression behavior over the range 0−7 GPa. This unusual behavior displayed by $RbNbWO_6$ and NH_4NbWO_6 is caused by the insertion of water molecules present in the hydrostatic fluid into the pyrochlore framework and accompanied by a shift of the A^+ cation to a smaller site within the pyrochlore channel structure. The volume expansion is a response to the overbonding of the A^+ cation on this new site.

Acknowledgment. Research carried out in part at the National Synchrotron Light Source at Brookhaven National Laboratory is supported by the U.S. Department of Energy (Contract No. DE-AC02-98CH10886 for beamline X7A). We gratefully acknowledge the Geophysical Laboratory of the Carnegie Institute for access to their ruby laser system at beamline X17C. P.W.B. and P.M.W. acknowledge the National Science Foundation (Grant No. 0094271) and The Ohio State University for support. Y.L. thanks the BNL-LDRD (Pressure in Nanopores), and J.A.H. acknowledges financial support from the Royal Society. We acknowledge Steven Bright of the Department of Materials Science and Engineering and Gordon Renkes of the Chemistry Department, both from The Ohio State University, for use of the Perkin-Elmer TG7 and Mattson Cygnus 100 FTIR instruments, respectively. P.W.B. thanks the Woodward Research Group for their helpful discussions during the duration of this work.

JA0292187

(33) Ionic radii are as follows: Rb^+, 1.66 Å (six-coordinate), 1.75 Å (eight-coordinate);[31] NH_4^+, 1.60−1.75 Å;[31,32] K^+, 1.52 Å (six-coordinate), 1.65 Å (eight-coordinate).[31]